MTSS1/Src family kinase dysregulation underlies multiple inherited ataxias

Alexander S. Brown[a,1], Pratap Meera[b], Banu Altindag[a], Ravi Chopra[c], Emma M. Perkins[d], Sharan Paul[e], Daniel R. Scoles[e], Eric Tarapore[f], Jessica Magri[a], Haoran Huang[c], Mandy Jackson[d], Vikram G. Shakkottai[c], Thomas S. Otis[g], Stefan M. Pulst[e], Scott X. Atwood[a,f,1], and Anthony E. Oro[a,1]

[a]Program in Epithelial Biology, Stanford University School of Medicine, Stanford, CA 94305; [b]Department of Neurobiology, University of California, Los Angeles, CA 90095; [c]Department of Neurology, University of Michigan, Ann Arbor, MI 48109; [d]Centre for Discovery Brain Sciences, University of Edinburgh, Edinburgh EH8 9XD, United Kingdom; [e]Department of Neurology, University of Utah Medical Center, Salt Lake City, UT 84132; [f]Department of Developmental and Cell Biology, University of California, Irvine, CA 92697; and [g]Sainsbury Wellcome Centre for Neural Circuits and Behavior, University College London, London WC1E 6BT, United Kingdom

Edited by Mary E. Hatten, The Rockefeller University, New York, NY, and approved November 1, 2018 (received for review September 18, 2018)

The genetically heterogeneous spinocerebellar ataxias (SCAs) are caused by Purkinje neuron dysfunction and degeneration, but their underlying pathological mechanisms remain elusive. The Src family of nonreceptor tyrosine kinases (SFK) are essential for nervous system homeostasis and are increasingly implicated in degenerative disease. Here we reveal that the SFK suppressor Missing-in-metastasis (MTSS1) is an ataxia locus that links multiple SCAs. MTSS1 loss results in increased SFK activity, reduced Purkinje neuron arborization, and low basal firing rates, followed by cell death. Surprisingly, mouse models for SCA1, SCA2, and SCA5 show elevated SFK activity, with SCA1 and SCA2 displaying dramatically reduced MTSS1 protein levels through reduced gene expression and protein translation, respectively. Treatment of each SCA model with a clinically approved Src inhibitor corrects Purkinje neuron basal firing and delays ataxia progression in MTSS1 mutants. Our results identify a common SCA therapeutic target and demonstrate a key role for MTSS1/SFK in Purkinje neuron survival and ataxia progression.

neurodegeneration | Src kinase | BAR domain proteins | spinocerebellar ataxia | actin cytoskeleton

Neurons are nondividing cells that depend on homeostatic regulation of protein, RNA, and metabolite turnover to permit dynamic synaptic connections that allow adaptation to changing environments. Loss of such mechanisms results in one of several hundred neurodegenerative disorders. Over 40 loci form the genetic basis for human spinocerebellar ataxia (SCA), a progressive motor disorder characterized by cerebellar atrophy and pervasive Purkinje neuron degeneration in which patients experience poor coordination and balance, hand–eye coordination, dysarthria, and abnormal saccades.

One common phenotype prominent in multiple SCA animal models is the altered Purkinje neuron firing rates that precede motor impairment and cell death (1–3), with restoration of the normal firing rates reducing Purkinje neuron death and improving motor function (4, 5). Defects in many cell functions, including effectors of transcription (6), translation (7), proteostasis (8, 9), calcium flux (10, 11), and cytoskeletal/membrane interactions (12, 13), lead to SCA. An open question that remains is how the many SCA genes interact to control firing rates and cell survival, with a common target emerging as an ideal treatment for the genetically diverse etiologies.

One such therapeutic target is the class of Src family of nonreceptor tyrosine kinases (SFKs). Several SFKs are expressed in the nervous system and have partially overlapping functions. While single mutants for *Src* or *Yes* kinase have no overt neuronal phenotype (14, 15), *Fyn* loss of function leads to increased Src activity and hippocampal learning and memory deficits (16, 17). Moreover, *Fyn;Src* double mutants rarely survive past birth and have severely disorganized cortical and cerebellar layers (15, 18). SFKs are posttranslationally regulated through activating and inhibitory phosphorylation marks deposited by inhibitory kinases and are removed by receptor tyrosine phosphatases in a context-dependent manner (19, 20). SFK activation occurs rapidly in response to extracellular signals and in response to a variety of cellular stressors ranging from osmotic pressure (21) to tetanic stimulation (22). Additionally, SFKs are inappropriately active in disease states including amyotrophic lateral sclerosis (23), Alzheimer disease (24), and Duchenne muscular dystrophy (25).

Missing-in-metastasis (MTSS1) is one of the defining members of the I-BAR family of negative membrane curvature-sensing proteins first identified as being deleted in metastatic bladder cancer (26). Although MTSS1 biochemically interacts with membranes and regulates the actin cytoskeleton (27), genetic studies reveal that MTSS1 functions in an evolutionarily conserved signaling cassette to antagonize Src kinase activity (28, 29). Disruption of the MTSS1/Src regulatory cassette results in endocytosis and polarization abnormalities demonstrated by defects in primary cilia-dependent hedgehog signaling, and hair follicle epithelial migration (28). In tissues requiring MTSS1 function, levels of active MTSS1 are critical, as loss (26) or gain (30) of MTSS1 has been associated with metastasis and invasion. Regardless of the particular phenotype, an evolutionarily conserved property of MTSS1 mutants is that loss of MTSS1 function can be reversed through

Significance

The Src family of nonreceptor tyrosine kinases (SFK) is essential for nervous system function and may contribute to neurodegeneration. Spinocerebellar ataxias (SCAs) are neurodegenerative diseases in which Purkinje neurons fire irregularly and degenerate leading to motor problems. We show that the SFK suppressor Missing-in-metastasis (MTSS1) is an ataxia gene that links multiple SCAs. MTSS1 loss results in increased SFK activity, degenerating Purkinje neurons with low firing rates, and cell death. Surprisingly, mouse models for three different SCAs show elevated SFK activity, with SCA1 and SCA2 models displaying dramatically reduced MTSS1 protein levels. Treatment of each SCA model with an SFK inhibitor corrects Purkinje basal firing and delays ataxia progression in MTSS1 mutants. Our results identify a common link among disparate neurodegenerative diseases.

Author contributions: A.S.B., P.M., M.J., V.G.S., T.S.O., S.M.P., S.X.A., and A.E.O. designed research; A.S.B., P.M., B.A., R.C., E.M.P., S.P., D.R.S., E.T., J.M., H.H., M.J., and S.X.A. performed research; A.S.B., P.M., R.C., E.M.P., S.P., D.R.S., M.J., V.G.S., T.S.O., S.M.P., S.X.A., and A.E.O. analyzed data; and A.S.B. wrote the paper.

The authors declare no conflict of interest.

This article is a PNAS Direct Submission.

Published under the PNAS license.

[1]To whom correspondence may be addressed. Email: sale@stanford.edu, satwood@uci.edu, or oro@stanford.edu.

This article contains supporting information online at www.pnas.org/lookup/suppl/doi:10.1073/pnas.1816177115/-/DCSupplemental.

Published online December 7, 2018.

the removal or inhibition of Src kinases. This property was demonstrated first through double-mutant analysis in the fly ovary and subsequently in mammalian tissue culture using Src family kinase inhibitors (28, 29). The availability of Food and Drug Administration (FDA)-approved Src kinase inhibitors has led to the investigation of clinically relevant MTSS1 phenotypes with the hope of using SFK inhibitors to ameliorate them.

Although SFKs have been shown to regulate multiple classes of neurotransmitter receptors (31), they also function to control basic cytoskeletal components. Src regulates local actin polymerization (32) and endocytic receptor internalization (32–35). The actin cytoskeleton plays a critical role in cell signaling, proliferation, motility, and survival. Local, rather than global, actin dynamics control homeostatic synaptic signaling, and abnormalities in actin regulation underlie a diversity of psychiatric and neuronal diseases including amyotrophic lateral sclerosis (36), schizophrenia, autism spectrum disorders (37), and motor dysfunctions such as SCA (38). Remaining major challenges are understanding how actin cytoskeletal regulation controls synaptic function and developing improved therapeutics for these common and poorly treated diseases.

Here we reveal that the actin regulator and SFK antagonist *Mtss1* is an ataxia locus regulated by multiple SCA alleles that subsequently result in SFK hyperactivation. We show that clinically available Src inhibitors correct Purkinje neuron firing rates and delay ataxia progression, demonstrating a druggable role for the evolutionarily conserved MTSS1/SFK network in Purkinje neuron survival and ataxia progression.

Results

Mtss1-Null Mice Display a Progressive Ataxia. Mtss1 functions in many tissues, and previous mutant alleles disrupting 5′ exons resulted in mild lymphomagenesis (39), progressive kidney disease (40), mild neurological phenotypes (41), and cerebellar dysfunction (42). However, *Mtss1* has several possible internal promoters (43), and multiple splice variants with differing subcellular localization (44) and existing mutant lines display MTSS1 proteins (40, 45). As an alternative approach, we generated a conditional mutant allele targeting the endophilin/Src-interacting domain located in the final exon (MIM^{Ex15}) (Fig. 1*A*) (28, 29). Germline deletion with HPRT-cre resulted in the loss of MTSS1 protein as detected by an antibody specific to the N-terminal I-BAR domain (Fig. 1*B*) (30).

To our surprise, homozygous MIM^{EX15} mutants appear normal for cilia-dependent processes with no observed instances of holoprosencephaly or polydactyly after multiple generations. Additionally, MIM^{EX15}-mutant males are fertile. Instead, MIM^{EX15} mutants display a striking and progressive ataxia. To better understand the nature of MIM^{EX15} ataxia, we characterized MIM^{EX15} mutants using an open field test to evaluate gross motor control. MIM^{EX15} mutants had reduced velocity (Fig. 1*C*) and rearing behavior (Fig. 1*D*), consistent with overall movement defects. To uncouple possible motor and behavioral abnormalities, we evaluated MIM^{EX15} mutants with a rotarod assay and observed coordination abnormalities as early as age 4 wk (Fig. 1*E*). Many spinocerebellar ataxias display progressive neurologic phenotypes. To determine whether MIM^{EX15} animals showed progressive deterioration, we employed a composite test

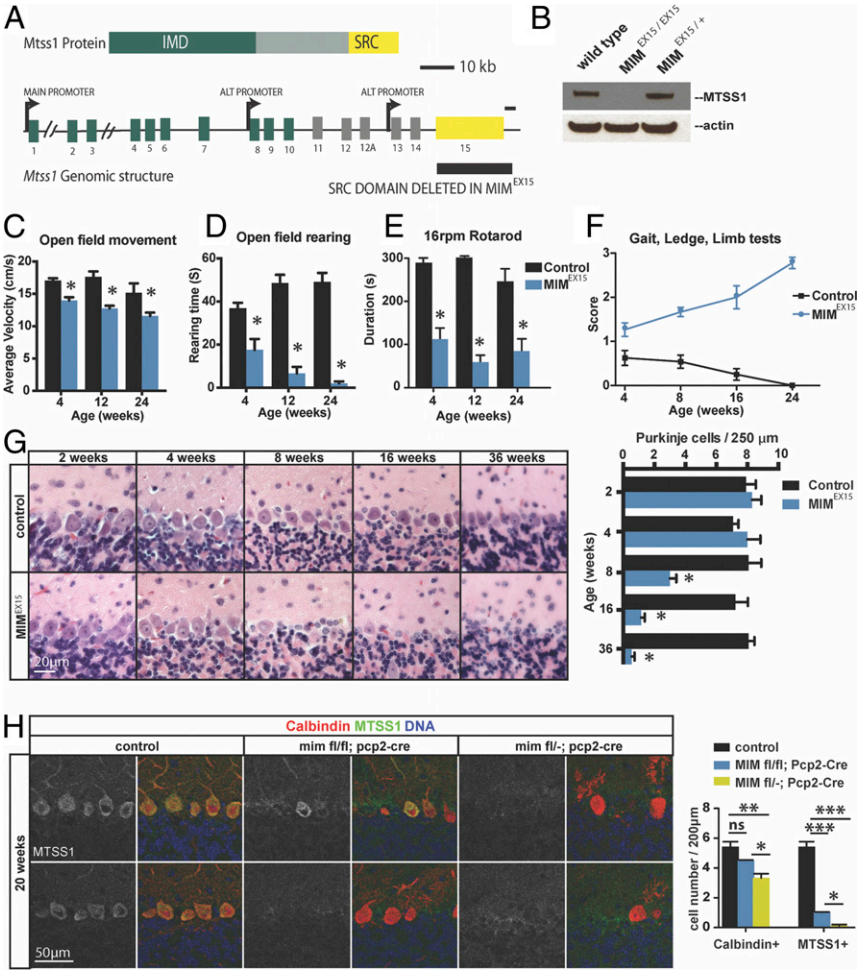

Fig. 1. MIM^{EX15} mutants develop progressive spinocerebellar ataxia. (*A*) The structure of the *Mtss1* locus with alternative promoters and the Src interacting domain deleted in MIM^{EX15} mutants. (*B*) Loss of MTSS1 protein in MIM^{EX15} cerebellum lysate shown with MTSS1 antibody against the N-terminal I-BAR (IMD) domain. (*C* and *D*) MIM^{EX15} mice show slower movement velocity (*C*) and less frequent rearing (*D*) in open field tests. (*E*) Impaired rotarod performance in MIM^{EX15} mutants is shown as reduced duration (time to fall). (*F*) A composite test of gait, balance, and grip strength to measure spinocerebellar ataxia symptoms. An increased score reflects reduced function with an age-dependent increase in severity in MIM^{EX15} mutants. (*G*) Age-dependent loss of Purkinje neurons in MIM^{EX15} mutants occurs after the onset of ataxia. (*H*) At 20 wk $MIM^{Loxp/-}$;Pcp2-Cre and $MIM^{Loxp/Loxp}$;Pcp2-Cre mutants show a dramatic reduction in Purkinje neurons that stain with MTSS1. Many Purkinje neurons persist, as there is a less dramatic reduction in calbindin^{+} Purkinje cell number. $^{*}P < 0.05$, $^{**}P < 0.005$, $^{***}P <$ 5E-5, one-way ANOVA with Tukey post hoc test; ns, not significant. Error bars indicate SEM.

measuring gait, grip strength, and balance (46). We found MIM^{EX15} animals performed consistently worse than controls, with severity increasing with age (Fig. 1*F*). MIM^{EX15}-heterozygous animals displayed 75% of normal protein levels (*SI Appendix*, Fig. S1*C*), giving no overt phenotype.

Reduced Mtss1 levels are associated with a variety of cellular phenotypes including reduced presentation of receptors on the cell membrane (47) and altered Purkinje neuron morphology (41, 44). To determine the basis of the motor abnormalities and to distinguish among these possibilities, we performed histological analysis. At age 4 wk, MIM^{EX15} mice are ataxic, but their cerebella appeared grossly normal with intact granule, Purkinje neuron, and molecular layers. However, MIM^{EX15} mutants displayed a progressive loss of Purkinje neurons in all cerebellar lobes, which was readily seen by 8 wk of age (*SI Appendix*, Fig. S1*A*). Wild-type cerebella contain approximately eight Purkinje neurons in a 250-μm linear distance, whereas 8-wk-old MIM^{EX15} mutants retained only 25% and 36-wk-old MIM^{EX15} mutants had only 5% of the total number of Purkinje neurons found in wild-type mice (Fig. 1*G*).

While ataxia genes can act in many cell types to regulate Purkinje cell function, MTSS1 is highly expressed in Purkinje cells, suggesting it is required in these cells for normal Purkinje cell function and survival. To confirm that the Purkinje neuron defects seen in MIM^{EX15} animals are due to a cell-autonomous requirement for *Mtss1*, we conditionally inactivated *Mtss1* using the Purkinje neuron-specific L7-Cre (MIM^{cko}) and then compared Purkinje neuron morphology and loss to that in the global MIM^{EX15} mutant. MIM^{cko} Purkinje neurons were mosaic for MTSS1 expression, likely due to inefficient LoxP recombination as the MTSS1 antibody showed high specificity (*SI Appendix*, Fig. S1*B*). At age 20 wk MIM^{cko} mice had a significant reduction in Purkinje neurons. In the remaining Purkinje neurons, those lacking MTSS1 protein displayed thickened dendritic branches and reduced arbor volume, while neighboring Purkinje neurons with MTSS1 protein appeared normal (Fig. 1*H*). We conclude that *Mtss1* acts cell autonomously to maintain dendritic structure in Purkinje neurons, with loss of MTSS1 resulting in abnormalities and eventual cell death.

Mtss1 Mutant Neurons Display Limited Autophagic Markers. An emergent mechanism of cell loss during neurodegeneration is aberrant macroautophagy. Autophagy is essential for Purkinje neuron survival, as loss of autophagy (48, 49) results in cell death. Increased levels of early autophagy markers have been described in multiple neurodegenerative diseases including Huntington's disease (50), Alzheimer disease (51), and SCA3 (52). MIM^{EX15} mutants partially fit this pattern of disease, as we observed some signs of autophagy. As early as age 4 wk, we observed increased complex V/ATP synthase staining indicative of fused mitochondria as well as dramatically reduced staining for the Golgi body marker giantin (Fig. 2*A*). We also observed increased transcript abundance for the early autophagy effector *VMP1* (53). By 8 wk of age, we could detect increased LC3-II species (Fig. 2*B* and *SI Appendix*, Fig. S2*A*), and electron microscopy revealed several autophagy-related morphologies, including swollen mitochondria, fragmented Golgi bodies, lamellar bodies, and double-membrane autophagic vacuoles (*SI Appendix*, Fig. S2*C*). Interestingly, we were unable to detect increased *Sqstrm1* (p62) transcript or protein levels in MIM^{EX15}, an autophagocytic adapter protein associated with protein aggregation in neurodegenerative disease (*SI Appendix*, Fig. S2*B*) (54). MIM^{EX15} animals displayed increased neuroinflammation shown by increased levels of Aif1 transcript, a readout of microglial infiltration (Fig. 2*D*). MIM^{EX15} animals also show increased $GFAP^{+}$ glial infiltration (Fig. 2 *E* and *F* and *SI Appendix*, Fig. S1*A*) consistent with reactive astroglyosis. Consistent with the signs of autophagocytic cell death and neuroinflammation, we failed to see increased DNA breaks in MIM^{EX15} Purkinje neurons with TUNEL staining (Fig. 2*G*).

Mtss1 Prevents SFK-Dependent Purkinje Neuron-Firing Defects and Ataxia. To characterize the cellular changes associated with the ataxia present in 4-wk-old MIM^{EX15} mice, we examined the dendritic tree of individual biocytin-injected Purkinje neurons (Fig. 3*A*). Purkinje neuron dendritic arbor collapse has been observed in several SCA models including SCA1 (2) and SCA5 (3), while many other models, including SCA2 (1) and SCA3 (55), have shown a thinned molecular layer that likely reflects reduced Purkinje dendritic volume. Similarly, MIM^{EX15} mutants showed a 60% reduction in the expansiveness of the dendritic tree (Fig. 3*B*) and a significant decrease in the number of dendritic spines (Fig. 3*C*), although no significant difference was detected in spine length (Fig. 3*D*) or width (Fig. 3*E*).

In dermal fibroblasts and *Drosophila* border cells MTSS1 functions locally to prevent ectopic Src kinase activity, and *Mtss1*-mutant phenotypes can be rescued by genetically removing Src kinase (28, 29). To determine if *Mtss1* acts similarly in Purkinje neurons, we evaluated SFK activity levels in cerebellar lysates from MIM^{EX15} mutants and found elevated levels of SFK^{Y416} (Fig. 3*F*) indicative of increased SFK activity. Previous work has shown strong functional interactions between SFK and metabotropic glutamate receptor type I (mGluR1) neurotransmission at parallel fiber (PF) synapses (56). To investigate whether MTSS1/SFK modulation of mGluR1 signaling forms the basis of the ataxia, we performed electrophysiological analysis of Purkinje neurons in cerebellar slices from MIM^{EX15} mice. We evaluated Purkinje neuron response to PF stimulation using calcium imaging. We found MIM^{EX15}-mutant Purkinje neurons responded with an increase of calcium-dependent fluorescence comparable to that in controls, while adding the mGluR1 antagonist CPCCOEt abolished these responses (Fig. 3*G*). These data support MTSS1 acting downstream of glutamate receptors to control Purkinje cell function.

Purkinje neurons maintain a cell-autonomous tonic firing rate that is essential for their function (57, 58). Since MIM^{EX15} Purkinje neurons responded normally to PF stimulation, suggesting normal synaptic transmission, we assayed the basal firing rate. The Purkinje neuron tonic firing rate is highly sensitive to temperature and may vary slightly with experimental conditions (59). In our assays, wild-type cells had a mean firing rate of 43 ± 2 Hz (n = 2 animals, 62 cells), while 4-wk-old MIM^{EX15} mutants exhibited a mean firing rate of 12 ± 1 Hz (n = 2 animals, 55 cells) (Fig. 3 *H* and *I*). Previous studies of SCA mouse models demonstrated that reduced tonic firing is a basis for ataxia (1, 3, 5). Since basal firing is reduced at an age when MIM^{EX15} mice possess a normal number of Purkinje neurons, our results suggest neuron malfunction rather than neuron loss underlies the initial ataxia phenotype.

MTSS1/Src double mutants rescue MTSS1 phenotypes in *Drosophila* and vertebrate cell culture. To test the hypothesis that reducing SFK activity would ameliorate the MIM^{EX15} ataxia phenotype, we added the FDA-approved SFK inhibitor dasatinib to cerebellar slice preparations using a concentration approximately twofold over the in vivo IC_{50} concentration (200 nM) and measured the basal firing rate (Fig. 3 *H* and *I*). Dasatinib significantly increased the MIM^{EX15} basal firing rate from baseline to 29 ± 1 Hz (n = 2 animals, 62 cells). We also observed that dasatinib slightly reduced the wild-type basal firing rate to 35 ± 1 Hz (n = 2 animals, 79 cells). Time-course experiments showed the increase in basal firing rate occurred over 5 h (*SI Appendix*, Fig. S3), consistent with a low-concentration, high-affinity mechanism of action. Direct modulation of ion channel or mGluR1 activity raises basal firing within minutes (4, 60), suggesting that dasatinib works through a distinct mechanism. To determine whether SFK inhibition ameliorates ataxia in vivo, we administered dasatinib directly to the cerebellum via minipumps to overcome poor CNS bioavailability (61). Over 4 wk, dasatinib-treated MIM^{EX15} mice

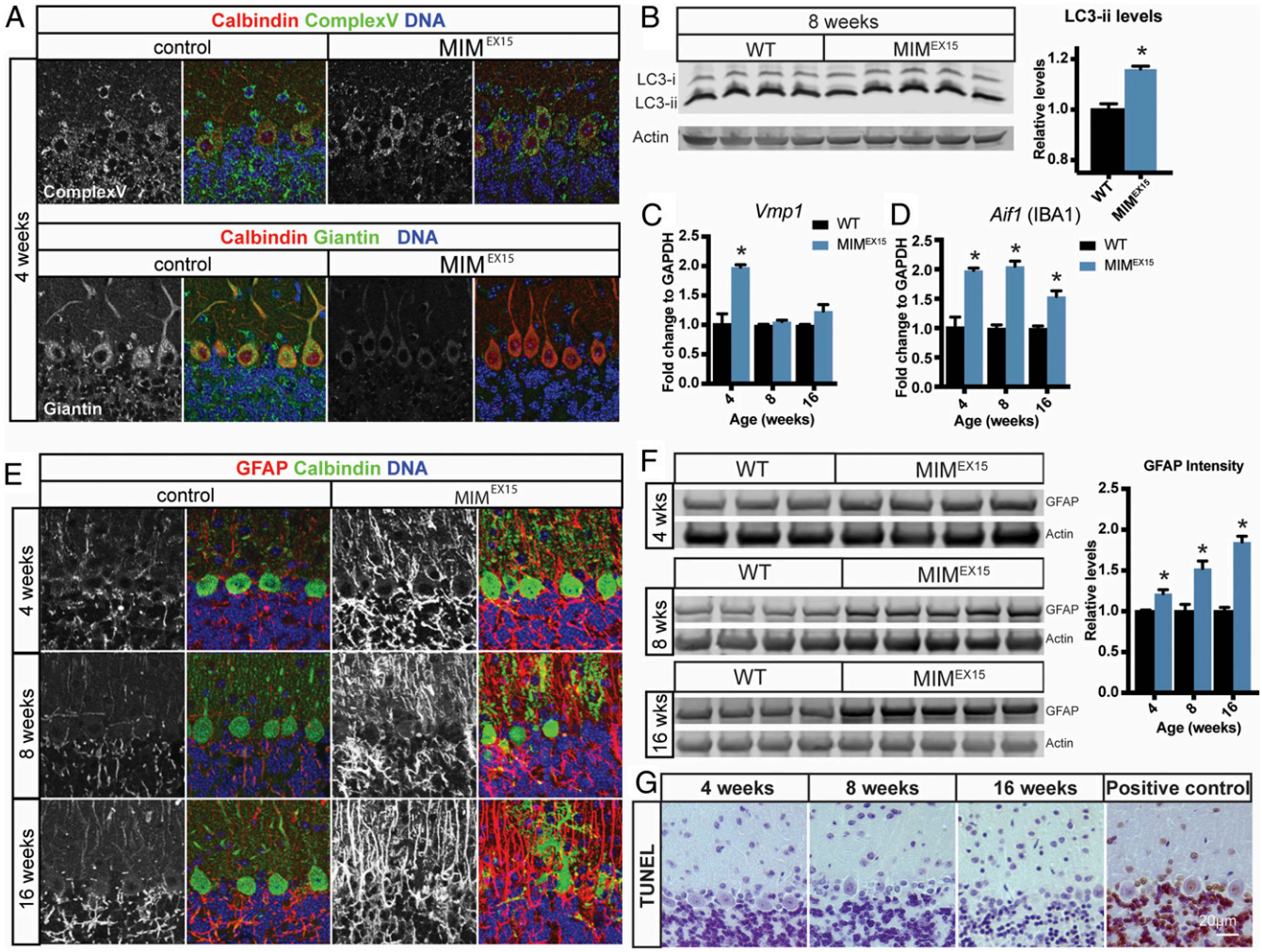

Fig. 2. *MIM*^{EX15}-mutant Purkinje neurons undergo autophagy. (*A*) *MIM*^{EX15} mutants display fused mitochondria shown by increased complex 5 ATP-synthase immunostaining and collapsed Golgi shown by reduced giantin immunostaining at 4 wk. (*B*) Eight-week-old *MIM*^{EX15} mutants show increased LC3-II abundance. *$P < 0.005$; Student's *t* test. (*C*) *MIM*^{EX15} mutants show increased levels of mRNA for the autophagocytic marker *VMP1*. *$P < 0.05$; Student's *t* test. (*D*) MIM^{EX15} mutants show increased microglial infiltration shown by *Aif1* transcript. *$P < 0.002$; Student's *t* test. (*E*) MIM^{EX15} mutants show GFAP^{+} glial infiltration during disease progression. (*F*) Western blots quantifying increased cerebellar GFAP. *$P < 0.05$; Student's *t* test. (*G*) MIM^{EX15}-mutant cerebella do not have increased TUNEL staining at 4, 8, or 16 wk of age.

were protected from disease progression while untreated mice showed progressively worsening rotarod performance ($n = 2$ dasatinib-treated mice and 3 control mice) (Fig. 3*J*). These results demonstrate that Src family kinases act downstream of MTSS1 and that SFK inhibitors rescue *Mtss1*-dependent basal firing rate defects to slow disease progression.

***Mtss1* Is a Translation Target of ATXN2.** The slow basal firing and ataxia preceding cell death seen in the MIM^{EX15} mutants resembles that seen in other SCA models such as SCA1, SCA2, and SCA5, prompting us to investigate whether MTSS1/SFK dysregulation occurs in other ataxias. SCA2 is caused by an expansion in the polyglutamine (polyQ) tract of the RNA-binding protein ATAXIN-2 (ATXN2) to more than 34 repeats (62). The exact molecular defects that drive SCA2 pathogenesis remain unclear, as mice with loss of ATXN2 function do not recapitulate the SCA2 phenotype (63), while intermediate-expansion alleles are associated with increased risk for ALS (64). Atxn2 has an ancestral role in translation control (7, 65), which may be altered with the SCA2 mutation, but the exact targets have yet to be described.

MTSS1 protein abundance is heavily regulated by metastasis-associated miRNAs, which bind to the *Mtss1* 3′ UTR and reduce steady-state MTSS1 protein levels (66–70). To determine whether MTSS1 protein accumulation is sensitive to Atxn2, we examined the *ATXN2*^{Q127} mouse model of SCA2 (1). We found MTSS1 abundance was progressively reduced by 90% at 24 wk, a level far greater than the 50% reduction in the Purkinje neuron marker calbindin (Fig. 4*A* and *SI Appendix*, Fig. S4). Cerebellar SFK activity was increased nearly eightfold in *ATXN2*^{Q127} animals compared with wild-type littermates (Fig. 4*B*).

We sought to determine whether the age-dependent reduction in Purkinje neuron basal firing frequency seen in *ATXN2*^{Q127} mice is due to elevated SFK activity. Remarkably, the addition of dasatinib to *ATXN2*^{Q127} cerebellar slices restored the basal firing rate from an average of 14 ± 1 Hz ($n = 2$ animals, 100 cells) to nearly normal levels of 32 ± 2 Hz ($n = 2$ animals, 72 cells) (Fig. 4 *C* and *D*). As in the MIM^{EX15} mutants, the firing rate reached maximal effect at 5–6 h of SFK inhibition (*SI Appendix*, Fig. S3), leading us to conclude that inappropriate SFK activity underlies both the ATXN2- and MTSS1-mediated firing phenotype.

The convergence of *Mtss1* and ATXN2 on SFK activity suggested they work in a common or parallel molecular pathway. To distinguish between these possibilities, we further interrogated MTSS1 protein levels in *ATXN2*^{Q127} cerebella. While we found

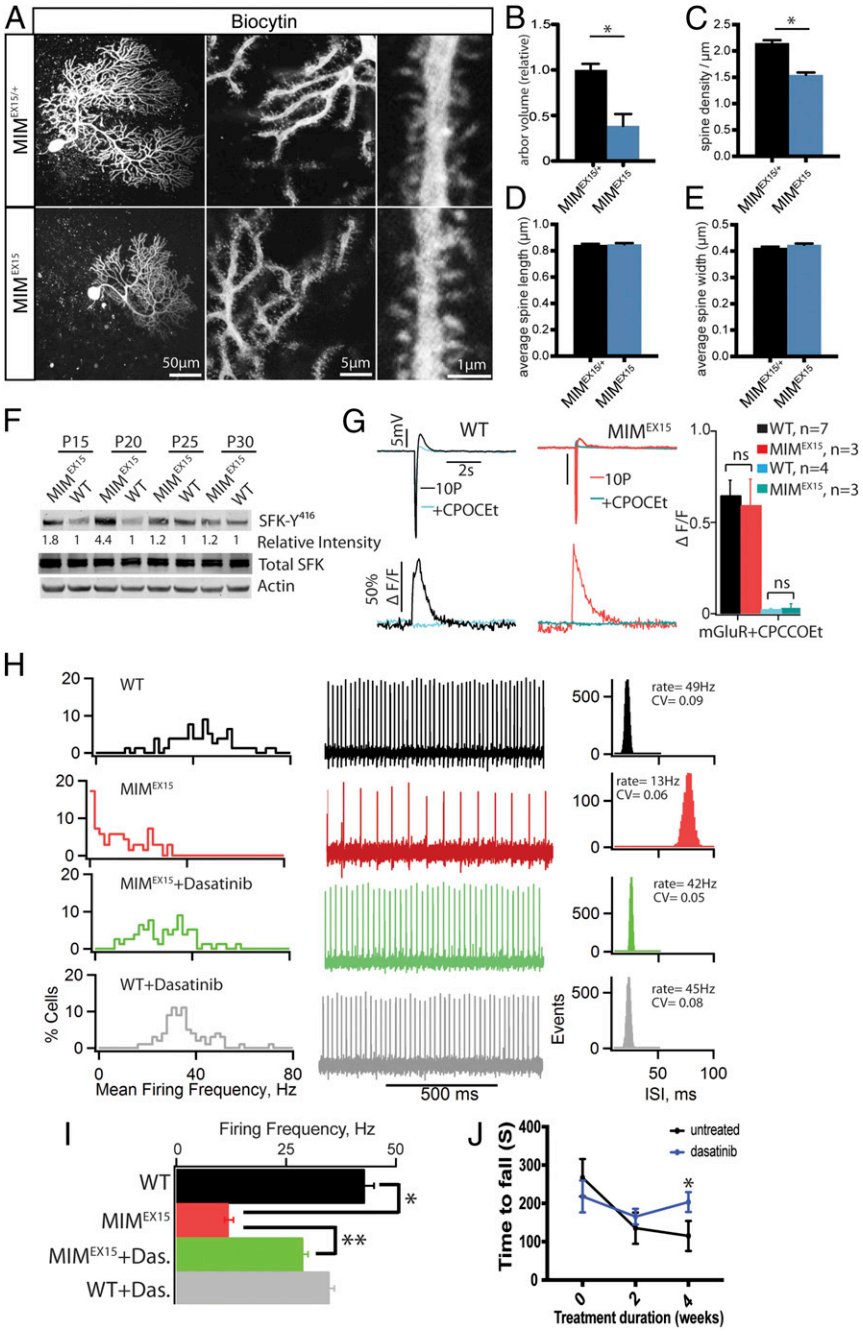

Fig. 3. Mtss1 prevents SFK-dependent firing defects and ataxia. (*A*) Confocal projection of an individual Purkinje cell filled with biocytin and fluorescent dye to visualize morphology. (*B–E*) Measurement of dye-filled Purkinje neurons shows MIM^{EX15} mutants have reduced arbor volume ($n = 3$ each genotype) (*B*) and reduced dendritic spine density (*C*) but no change in dendritic spine length (*D*) and no change in dendritic spine width (*E*). $MIM^{EX15/+}$, $n = 3$ neurons, 1,720 spines; MIM^{EX15}, $n = 3$ neurons, 1,454 spines. $^*P < 0.05$, Student's *t* test. Error bars indicate SEM. (*F*) Western blot for active SFK-Y416 phosphorylation with actin as a loading control. Cerebellar lysate was collected from MIM^{EX15} mice and age-matched controls at the indicated times between postnatal day 15 (P15) and postnatal day 30 (P30). (*G*) Slow EPSP in wild-type (*Left*) and MIM^{EX15} (*Center*) cells elicited by the stimulation of parallel fibers with 10-pulse trains at 100 Hz in the presence AMPA, NMDA, and GABA receptor antagonists (control conditions). Corresponding intracellular Ca^{2+} signals (ΔF/F) for responses for wild-type and MIM^{EX15} mGluR EPSPs are illustrated. EPSPs and corresponding Ca^{2+} signals are blocked by mGluR1 antagonist CPCCOEt. (*Right*) Summary data of intracellular Ca^{2+} signals (ΔF/F) for responses for WT and $MTSS1^{EX15}$ in control conditions and in the presence of CPCCOEt are shown. (*H*) Percent histograms of Purkinje neuron mean firing frequencies (*Left*), examples of extracellular recordings of 1-s duration of a spontaneously spiking Purkinje neuron in the respective condition (*Center*), and histograms of interspike intervals (ISIs) calculated for the 2-min recording periods of the same neuron (*Right*) are shown for the wild-type, MIM^{EX15}, wild-type+dasatinib, and MIM^{EX15}+dasatinib conditions. (*I*) Summary of data presented in *H*. $^*P = 6.1E\text{-}14$; $^{**}P = 1E\text{-}13$; one-way ANOVA, Tukey post hoc test. (*J*) Direct cerebellar administration of dasatinib maintains rotarod performance, slowing the progressive ataxia in MIM^{EX15} mice. $q = 0.006$, two-stage step-up Benjamini, Krieger, Yekutieli method. Error bars indicate SEM.

reductions of MTSS1 protein (*SI Appendix*, Fig. S4*A*) and RNA in $ATXN2^{Q127}$ Purkinje neurons (*SI Appendix*, Fig. S4*B*), we failed to see comparable changes in ATXN2 levels in 4-wk-old MIM^{EX15} mice (Fig. 4*E*). Because ATXN2 possesses RNA-binding activity, and *Mtss1* contains a long 3′ UTR, we hypothesized that ATXN2 controls *Mtss1* translation in Purkinje neurons. RNA-immunoprecipitation followed by qPCR in cells expressing tagged versions of either WT ($ATXN2^{Q22}$) or SCA2 ($ATXN2^{Q108}$) demonstrated both proteins specifically bound *MTSS1* mRNA compared with the *GAPDH* control (Fig. 4*F*). Using a luciferase reporter fused to the *MTSS1* 3′ UTR, we were able to map the ATXN2-interacting domain to a central 500-bp region that was sufficient for both RNA–protein interaction and translation control (*SI Appendix*, Fig. S4 *C* and *D*). Furthermore, polyribosome fractionation experiments revealed that pathogenic $ATXN2^{Q108}$ was sufficient to block the translation of reporter mRNA fused to the *MTSS1* 3′ UTR, shifting the transcript from the polyribosome fractions to a detergent-resistant fraction consistent with stress granules (Fig. 4*G*). These results suggest the pathogenic ATXN2 acts directly as a dominant-negative RNA-binding protein preventing MTSS1 translation. Notably, we observed MTSS1 abundance is reduced in the cerebellum of human SCA patients, bolstering the evolutionary conservation of the ATXN2/MTSS1 interaction (Fig. 4*H*).

SFK Inhibition Rescues Purkinje Neuron Firing Across SCA Models. Two other SCA mouse models, SCA1 (2) and SCA5 (3), have been shown to have slow basal firing rates. Much like SCA2, SCA1 is due to a polyQ expansion in the RNA-binding protein ATAXIN-1 (ATXN1) (71). One observed result of the SCA1 allele is changed ATXN1 association with transcriptional regulatory complexes (72), leading to vastly different Purkinje

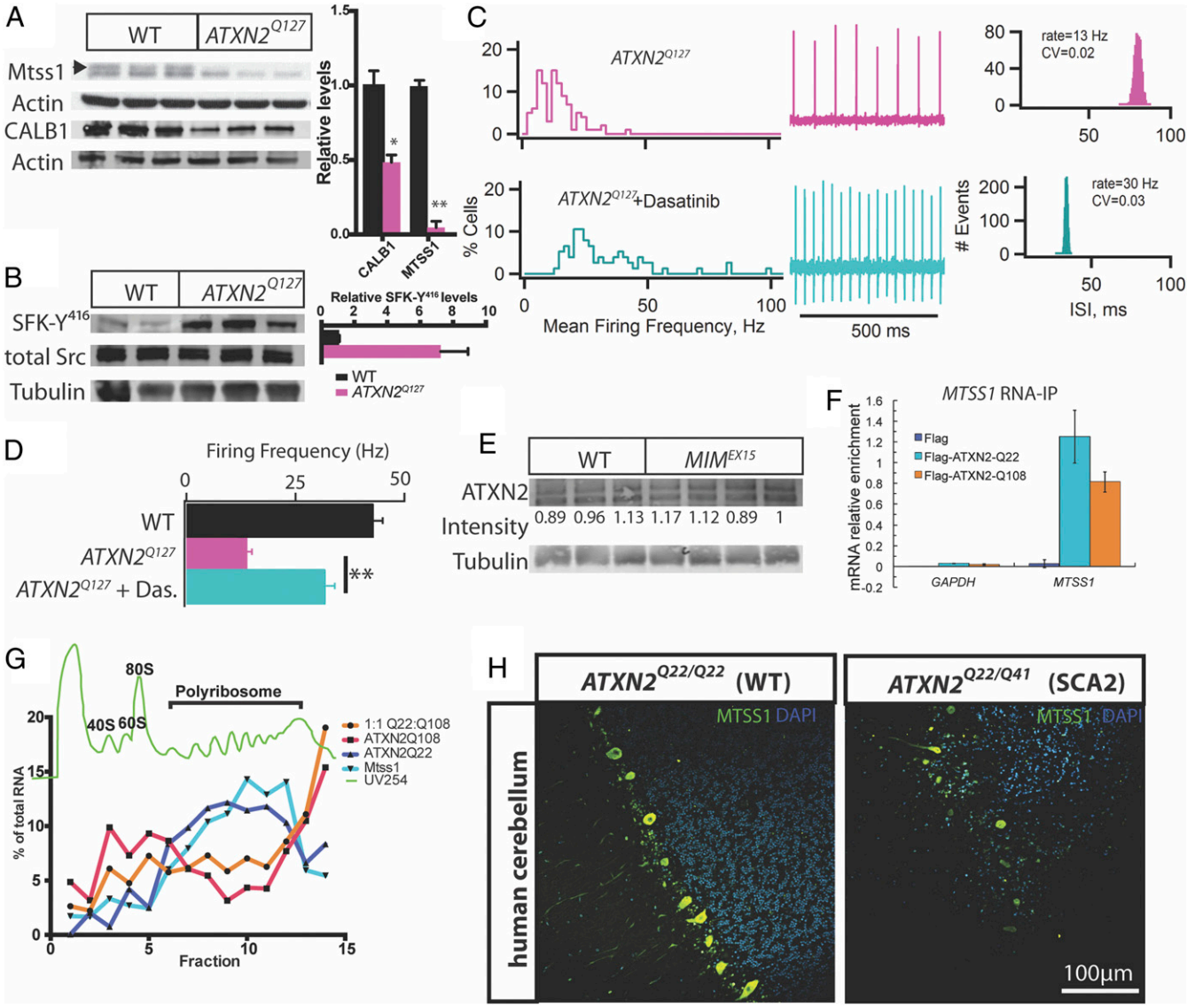

Fig. 4. MTSS1 is an ATXN2 translation target. (*A*, *Left*) Western blot of whole-cerebellum lysate from 24-wk-old mice shows 90% reduction (arrow) in the band that corresponds MTSS1 in *ATXN2*^{Q127} mice, while calbindin (CALB1) was reduced 50%. Actin is included as a loading control. (*Right*) Quantitation of Western blot results. *$P < 0.01$, **$P < 0.001$; Student's *t* test. (*B*, *Left*) Western blots for active SFK-Y416 phosphorylation and total Src in cerebellar lysate from 24-wk-old Atxn2^{Q127} mice show an eightfold increase in SFK-Y416 abundance. Tubulin was used as a loading control. (*Right*) Quantitation of Western blot results. (*C*) Percent histograms of Purkinje neuron mean firing frequencies (*Left*), examples of extracellular recordings of 1-s duration of a spontaneously spiking Purkinje neuron in the respective condition (*Center*), and histograms of interspike intervals calculated for the 2-min recording periods of the same neuron for *ATXN2*^{Q127} and *ATXN2*^{Q127}+dasatinib. (*D*) Mean firing rates. **P = 3.77E-8; one-way ANOVA and Tukey post hoc test. (*E*) Western blot for Atxn2 in cerebellar lysate from 4-wk-old *MIM*^{EX15} cerebellum and age-matched controls with tubulin as a loading control. (*F*) RNA-immunoprecipitation in HEK-293 cells for Flag-ATXN2^{Q22} and Flag-ATXN2^{Q108} shows enrichment for *MTSS1* but not *GAPDH* mRNA. Error bars indicate SD. (*G*) Polyribosome fractionation in 293T cells transfected with the MTSS1 UTR reporter and pcDNA, ATXN2^{Q22}, ATXN2^{Q108}, or ATXN2^{Q22}+ATXN2^{Q108}. The green line indicates UV 254-nm absorbance (nucleic acids) with 40S, 60S, 80S, and polyribosome peaks labeled. (*H*) Remaining Purkinje neurons in human SCA2 cerebellum (*ATXN2*$^{Q22/Q41}$) show reduced MTSS1 staining compared with an age-matched control (*ATXN2*$^{Q22/Q22}$).

neuron mRNA profiles (73). However, the exact targets that drive SCA1 pathogenesis are still being determined. Unlike SCA1 and SCA2, SCA5 is a more pure cerebellar ataxia due to lesions in the structural protein β-III spectrin (13). β-III spectrin directly binds to and controls the cell membrane localization of EAAT4 (excitatory amino acid transporter 4), a protein involved in the synaptic clearance of glutamate (12, 74).

If SCA1 or SCA5 arises similarly to SCA2 by dysregulation of the MTSS1/SFK cassette, we would expect decreased MTSS1 abundance. Indeed, in the *ATXN1*^{Q82} mouse model of SCA1 (75) we observed a 95% decrease in MTSS1 protein abundance (Fig. 5*A*) with only a 50% reduction in calbindin, suggesting the loss of MTSS1 is not solely due to the loss of Purkinje neurons.

Atxn1 pathogenicity is partially driven by phosphorylation at serine776 (72), which was unchanged in 4-wk-old *MIM*^{EX15} mice, suggesting that MTSS1 is a target of the SCA1 allele (Fig. 5*B*). Additionally, *Mtss1* transcript abundance is reduced at multiple ages in *ATXN1*^{Q82} mice (Fig. 5*C*) (73). We found treating *ATXN1*^{Q82} slices with dasatinib increased the basal firing rate from a baseline of 15 ± 1 Hz (n = 3 animals, 21 cells) to 23 ± 2 Hz (n = 3 animals, 21 cells), a level statistically indistinguishable from dasatinib-treated controls (Fig. 5*D*).

By contrast, the *Sptbn2*-knockout model of SCA5 (βIII spectrin$^{-/-}$) (3), showed no change in MTSS1 protein abundance at 3 wk but demonstrated a clear increase in SFK^{Y416} phosphorylation (Fig. 5*E*). We also observe increased basal firing from 25 ± 1 Hz (n = 2 animals, 31 cells) to 30 ± 2 Hz (n = 3 animals, 43 cells) over a 7-h period of dasatinib treatment (Fig. 5*F*). We failed to see changes in β-III spectrin abundance in *MIM*^{EX15} mice and detected a 40% decrease in β-III spectrin levels in 24-wk-old *ATXN2*^{Q127} mice that is likely due to reduced Purkinje neuron dendritic arbor size, correlating with calbindin levels (Fig. 5 *G* and *H*). Together these data suggest that β-III spectrin and MTSS1 may work in parallel, through different mechanisms, to modulate SFK activity (Fig. 5*I*).

Discussion

While SCA gene functions appear heterogeneous, our study establishes a genetic framework to understand how several SCA loci regulate SFK activity to ensure neuronal homeostasis and survival. We identify β-III spectrin and MTSS1, proteins that link the cell membrane and actin cytoskeleton, as negative regulators of Src family kinases. We show that MTSS1 is a target of the SCA genes *ATXN1* and *ATXN2* (Fig. 5*I*), and that increased SFK activity from lesions in *MTSS1*, *SPTNB2* (SCA5), *ATXN1* (SCA1), and *ATXN2* (SCA2) reduces Purkinje neuron basal firing, an endophenotype that underlies multiple ataxias, providing support for the clinical use of SFK inhibitors in many SCA patients.

Our results reveal a central role for the MTSS1/SFK regulatory cassette in controlling neuronal homeostasis and survival. MTSS1 regulation of SFKs has been demonstrated in several migratory cell types, including metastatic breast cancer and *Drosophila* border cells. Here we demonstrate the regulatory cassette functioning in nonmigratory postmitotic cells. MTSS1 integrates the cell membrane and cytoskeletal response to local

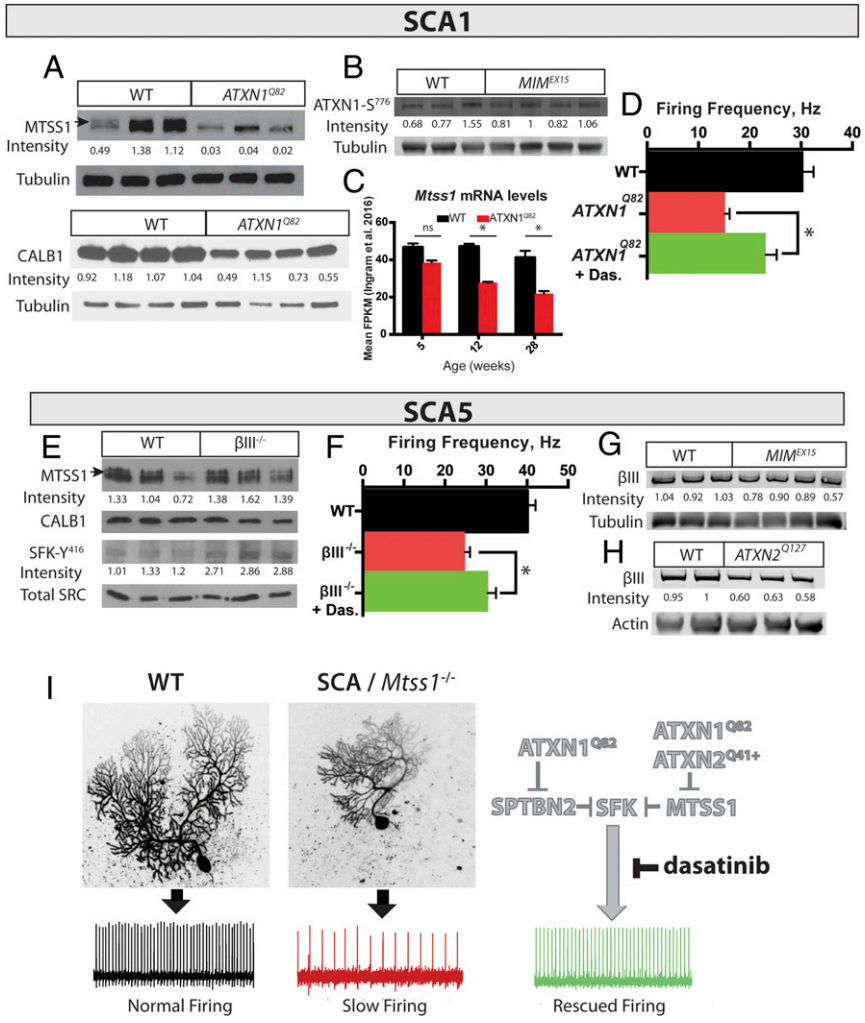

Fig. 5. SFK dysregulation occurs in multiple SCAs. (*A*) Western blot of whole-cerebellum lysate from 15-wk-old mice shows a 95% reduction of in the band that corresponds to MTSS1 in *ATXN1*^{Q82} mice but only a 50% reduction in calbindin. Tubulin is included as a loading control. (*B*) Western blot of cerebellum lysate from 4-wk-old MIM^{EX15} mice shows no change in phospho-serine776 ATXN1 levels. (*C*) RNA-sequencing from *ATXN1*^{Q82} cerebella shows reduced fragments per kilobase of transcript per million mapped reads for *Mtss1* mRNA in samples from 12-wk-old and 28-wk-old mice (*$q < 0.005$). (*D*) Mean firing frequency values (in Hertz) for WT and *ATXN1*^{Q82} mice, with and without dasatinib (Das) treatment. *$P = 0.0094$, one-way ANOVA with Tukey post hoc test. Error bars indicate SEM. (*E*) Western blot of whole-cerebellum lysate from 3-wk-old mice shows no change in MTSS1 in βIII-spectrin$^{-/-}$ mice, but active SFK-Y416 phosphorylation is increased. Calbindin and total Src are included as loading controls. (*F*) Mean firing frequency values (in Hertz) for wild-type and βIII-spectrin–/– mice, with and without dasatinib treatment. *$P < 0.05$, one-way ANOVA, Tukey post hoc test. Error bars indicate SEM. (*G*) SPTNB2 abundance is not changed in 4-wk-old MIMEX15 mice. (*H*) βIII-spectrin levels are reduced 40% in 24-wk-old *ATXN2Q127* mice. (*I*) A model in which pathogenic alleles of ATNX1 (ATXN1^{Q82}) and ATXN2 (ATXN2^{Q42}) prevent the accumulation of MTSS1 and SPTBN2 which restrain SFK activity to prevent abnormal firing patterns and neurodegeneration.

signals by serving as a docking site for the kinases and phosphatases that control actin polymerization (76), a process essential for dendritic spine assembly, maintenance, and function. In fly border cells, MTSS1-regulated SFK activity polarizes the membrane to spatially detect guidance cues. Similarly, MTSS1 functions in neurons to promote dendritic arborization and spine formation, structures that were shown to be essential for maintaining basal firing frequencies, by electrically isolating increasing areas of Purkinje neuron dendrites (59). Other members of the I-BAR family of membrane/cytoskeletal signaling proteins have been implicated in human neurological disorders such as microcephaly (77), but how they interact with MTSS1 remains to be determined.

Disruption of posttranscriptional gene regulation leading to altered proteostasis has recently emerged as a key contributor to neurodegeneration. In the cerebellum, reducing the abundance of the RNA-binding protein Pumilio leads to SCA1-like neurodegeneration through a specific increase in ATXN1 protein levels (78, 79). However, Pumilio binds hundreds of transcripts to control protein levels (80, 81), suggesting that changing the protein abundance of a few key effector genes posttranscriptionally leads to disease. Our data demonstrate that *MTSS1* is a key effector gene whose activity is tightly regulated to prevent Purkinje neuron malfunction. Posttranscriptional control of MTSS1 is disrupted in many disease states such as cancer, where MTSS1 levels are reduced by locus deletion or miRNA overexpression and are associated with increased metastasis and poorer prognosis (67, 82). In Purkinje neurons, the SCA1 $ATXN1^{Q82}$ allele reduces MTSS1 transcript levels. ATXN1 is thought to act as a transcriptional regulator by associating with the transcriptional repressor *Capicua* (CIC) (72), although whether the ATXN1/CIC complex occupies the *MTSS1* promoter remains to be shown. By contrast, the SCA2 allele $ATXN2^{Q108}$ binds the MTSS1 3′ UTR to prevent ribosome binding and MTSS1 translation, ultimately leading to increased SFK activity. ATXN2 (and the redundant protein ATXN2L) have recently been identified in a large complex of 3′ UTR-binding proteins that regulates networks of genes controlling epithelial differentiation and homeostasis (83). Our results suggest other ataxia disease genes that control proteostasis may also regulate MTSS1 abundance, and the strong role for miRNAs in controlling MTSS1 abundance in cancer suggests they may also function as effectors of as yet undescribed ataxia loci.

The identification of the MTSS1/SFK regulatory cassette in multiple ataxias further reinforces the pathological consequences associated with inappropriate SFK activation in response to a variety of cellular stresses. While the cytoskeletal regulator MTSS1 is an evolutionarily conserved SFK inhibitor, SFK effects on Purkinje neuron basal firing may derive from the fundamental roles SFKs play in cell homeostasis outside cytoskeletal control. For example, SFK control of translation is implicated in Alzheimer disease, as reducing SFK activity proves beneficial for Alzheimer disease progression (24) due to SFK control of pathogenic Aβ translation (84). SFK impairment of autophagy is seen in models of amyotrophic lateral sclerosis and Duchenne muscular dystrophy (23, 25). Additionally, reduction of Src kinase expression was identified as a suppressor of SCA1 toxicity in *Drosophila* ommatidia (85), supporting the need for moderating SFK activity. The pleiotropic effects of inappropriate SFK activity suggest that SFK inhibition may be a critical therapeutic node to slow the progression of multiple neurodegenerative disorders including SCAs. Our work points out the need for future development of neuroactive SFK inhibitor variants, as currently approved Src inhibitors were designed for oncology targets and lack potent CNS activity. Further, while we provide data showing that kinase inhibition suppresses MTSS1 loss, we have previously shown that SFK regulation by regulatory receptor tyrosine phosphatases or the deletion of endocytic adapter proteins can also revert the effects of MTSS1 loss. Given the challenge of developing specific kinase inhibitors, our work opens additional therapeutic classes to alleviate the progression of neurodegenerative diseases.

In summary, the identification of *Mtss1* as a recessive ataxia locus extends the physiologic functions requiring the MTSS1/SFK signaling cassette, which include cell polarity, migration, and cancer metastasis. Each of these disparate processes highlights the common role MTSS1 plays in integrating the cell membrane and cytoskeletal response to local signals, as the dendritic spine defects seen in MIM^{EX15}-mutant Purkinje neurons (Fig. 3 *A–E*) recall the loss of directional cell extensions in migrating *Drosophila* border cells (29). They also reinforce the critical need to suppress inappropriate SFK activity and provide a therapeutic opportunity for otherwise devastating and debilitating diseases.

Materials and Methods

Generation of the MIM^{EX15} Allele. To generate the MIM^{EX15} conditional allele, exon15 was cloned into the PGK-gb2 targeting vector between the 5′ LoxP site and the 3′ LoxP/FRT flanking neomycin cassette. The targeting vector contained a 5.97-kb 5′ homology arm that included exons 12, 13, and 14 and a 2.34-kb 3′ homology arm that included the 3′ UTR. The targeting vector was electroporated into C57bl6 × SV129 ES cells, and Neo-resistant colonies were screened by PCR. Chimeric mice were generated by injecting ES cells into blastocysts, and chimeras were mated to a FLP deleter strain (86). To generate MIM^{EX15}-null animals, mice with the MIM^{EX15} conditional allele were crossed to HPRT-Cre mice (87). Cerebellar-specific MIM deletion used the previously described PCP2-Cre line (88). Mice were maintained on a mixed C57bl6 SV129 background and were examined at the listed ages. All animals studies were approved by the Stanford APLAC Review Board #14126.

Western Blot. Isolated tissues were lysed in RIPA buffer supplemented with cOmplete mini protease inhibitor (Roche) and PhosSTOP (Roche). Protein concentrations were normalized by using the BCA assay (Pierce). Proteins were electrophoresed on Novex 4–12%, 3–8%, and 10–20% gradient gels or 16% gels. Rabbit anti-Src-Y416 (2101S or 6943S; Cell Signaling Technology), mouse anti–β-actin (Sigma), rabbit anti-Sptbn2 (PA1-46007; Thermo), rabbit anti-Atxn2 (HPA021146; Sigma), mouse anti-Atxn1 (ab63376; Abcam), rabbit anti-LC3A/B (4108; Cell Signaling Technology), rabbit anti-P62 (23214; Cell Signaling Technology), and rabbit anti-Src (2123 or 2108; Cell Signaling Technology) primary antibodies were detected with LICOR secondary antibodies.

Antibodies and Immunofluorescence. Isolated cerebella were immersion-fixed in 4% paraformaldehyde and embedded in paraffin. Seven-micrometer sections were cut and deparaffinized using standard conditions before staining. Sections were blocked with 20% horse serum and 0.3% Triton X-100 in PBS. The following antibodies were used at 1:1,000 dilutions: rabbit anti-Mtss1 (30), rabbit anti-calbindin (13176; Cell Signaling Technology), mouse anti–calbindin-D-28K monoclonal (Sigma), mouse anti-complex V (Novex; 459240), rabbit anti-ubiquitin (3933; Cell Signaling Technology), rabbit anti-giantin (Abcam; ab24586), and chicken anti-GFAP (ab4674; Abcam). Alexa-Fluor–conjugated secondary antibodies were purchased from Invitrogen. Images were acquired on a Leica SP2 laser-scanning microscope equipped with an acousto-optical beam splitter (AOBS) or a Zeiss Axioplan widefield microscope.

Human Samples. Paraffin-embedded brain slices from an SCA2 patient were provided by Arnulf H. Koeppen, Albany Medical College, Albany, NY. Non-SCA2 control paraffin-embedded brain slices were provided by Joshua Sonnen, University of Utah School of Medicine, Salt Lake City. Human tissues were maintained and processed under standard conditions consistent with NIH guidelines and conformed to an approved University of Utah Institutional Review Board protocol. Sections were deparaffinized using standard conditions, blocked/permeabilized with 5% donkey serum and 0.3% Triton X-100 in PBS, and processed for immunostaining. The nuclei were stained with DAPI followed by mounting with Fluoromount-G (catalog no. 0100-01; Southern Biotech). Antibody dilutions for tissue immunostainings were 1:500 for the custom-designed MTSS1 antibody and 1:1,000 for the fluorescent secondary antibody: goat anti-rabbit IgG (H + L) antibody, DyLight-488 (catalog no. 35552; Thermo Fisher Scientific). Images were acquired using a Nikon Eclipse Ti confocal microscope in the University of Utah Cell Imaging Core Laboratory and were analyzed by NIS-Elements AR 4.5 software. Because massive degeneration of cerebellum is seen in SCA2 brain tissue, the lobe cannot be verified.

Electrophysiology.

Preparation of SCA2 and Mtss1 cerebellar slices. Acute parasagittal slices of 285-μm thickness were prepared from the cerebella of 4- to 8-wk-old (MIM^{EX15}), or 24- to 29-wk-old ($ATXN2^{Q127}$) mutants and control littermates following published methods (1). In brief, brains were removed quickly and immersed in an ice-cold artificial cerebrospinal fluid (ACSF) solution or an extracellular solution consisting of 119 mM NaCl, 26 mM $NaHCO_3$, 11 mM glucose, 2.5 mM KCl, 2.5 mM $CaCl_2$, 1.3 mM $MgCl_2$, and 1 mM NaH_2PO_4, pH 7.4 when gassed with 5% CO_2/95% O_2. Cerebella were dissected and sectioned using a Leica VT-1000 vibratome. Slices were initially incubated at 35 °C for 35 min and then at room temperature before recording in the same ACSF. Dasatinib (200 nM) was added during cerebellar sectioning and remained on the slices for recording.

SCA2 and Mtss1 recordings. Noninvasive extracellular recordings were obtained from Purkinje neurons in voltage-clamp mode at 34.5 ± 1 °C. The temperature was maintained using a dual-channel heater controller (Model TC-344B; Warner Instruments), and slices were constantly perfused with carbogen-bubbled extracellular solution alone or with 200 nM dasatinib. Cells were visualized with an upright Leica microscope using a water-immersion 40× objective. Glass pipettes were pulled with a model P-1000 micropipette puller (Sutter Instruments). Pipettes had a 1- to 3-MΩ resistance when filled with extracellular solution and were used to record action potential-associated capacitative current transients near Purkinje neuron axon hillocks with the pipette potential held at 0 mV. Data were acquired at 20 kHz using a Digidata 1440 MultiClamp 700B amplifier, with pClamp10 (Molecular Devices), filtered at 4 kHz. A total of 50–100 Purkinje neurons were measured from each genotype; each recording was 2 min in duration. The experimenter was blinded to the mouse genotype; two to four mice were used per genotype. Simultaneous mGluR excitatory postsynaptic potentials (EPSPs) and calcium were measured in the presence of the $GABA_A$ receptor antagonist picrotoxin (PTX) (100 μM), and AMPA receptor blockers (5 μM NBQX and 10 μM DNQX) using a two-photon microscope and a standard electrophysiology set-up. The patch pipettes had a 4- to 5-MΩ resistance when filled with internal solution (135 mM $KMS0_4$, NaCl, 10 mM Hepes, 3 mM MgATP, and 0.3 mM Na2GTP) containing 200 μM Oregon Green Bapta1 and 20 μM Alexa-Fluor 594. The stimulating electrode was filled with ACSF containing 20 μM Alexa-Fluor 594 and was placed in the dendritic region to stimulate PF synaptic inputs minimally. Slow mGluR EPSPs in control littermates and mutants were elicited by stimulation of PFs with 100-Hz trains of 10 pulses in the presence of receptor antagonists that block AMPA, NMDA, and $GABA_A$ receptors. Corresponding intracellular Ca^{2+} signals (ΔF/F) for responses for wild-type and mutant mGluR EPSPs were blocked by the mGluR1 antagonist CPCCOET.

Experiments were analyzed using both the Clampfit and Igor algorithms and were further analyzed using Microsoft Excel. Figures were made in the Igor program. Calcium signals were analyzed using SlideBook (Intelligent Imaging Innovations, Inc.). Results are presented as mean ± SEM. All chemicals were purchased from Sigma Aldrich, Tocris, or Invitrogen.

Biocytin Fills of Purkinje Neurons or Intracellular Labeling of Purkinje Neurons with Biocytin. Biocytin filling of Purkinje neurons was performed using recording pipettes filled with 1% Biocytin (Tocris). Purkinje neurons were filled for 15–30 min; then the pipette was removed slowly to enable the cell membrane to reseal. Slices were fixed in 4% paraformaldehyde overnight and washed three times with PBS. Slices were then incubated with Alexa-Fluor 488 streptavidin (1:500, S11223; Thermo Fisher Scientific) in PBS, 0.5% Triton X-100, and 10% normal goat serum for 90 min. After another three PBS washes, the slices were mounted onto a slide with ProLong Gold (Thermo Fisher). Individual biocytin-filled Purkinje cells were visualized on a Leica SP2 AOBS laser-scanning microscope at a 0.5-um step size. Dendritic arbor volume was measured by calculating the biocytin-filled area in each confocal optical section using ImageJ (NIH), adding the areas in each z-stack, and multiplying by the step size.

ACKNOWLEDGMENTS. We thank JoAnn Buchanan for assistance with transmission electron microscopy, Hak Kyun Kim, Miguel Mata, and Peter Sarnow for assistance with ribosome profiling, and the Stanford Behavioral and Functional Neuroscience Laboratory for assistance with behavior assays. This work was funded by NIH Grants R01 AR052785 (to A.E.O.), F32 GM105227 (to A.S.B.), R37 NS033123 (to S.M.P.), R01 NS097903 (to D.R.S.), R21 NS103009 (to S.M.P. and D.R.S.), R01 NS085054 (to V.G.S.), and R01 NS090930 (to T.S.O.) and by The Wellcome Trust Grant 093077 (to M.J.).

1. Hansen ST, Meera P, Otis TS, Pulst SM (2013) Changes in Purkinje cell firing and gene expression precede behavioral pathology in a mouse model of SCA2. *Hum Mol Genet* 22:271–283.
2. Inoue T, et al. (2001) Calcium dynamics and electrophysiological properties of cerebellar Purkinje cells in SCA1 transgenic mice. *J Neurophysiol* 85:1750–1760.
3. Perkins EM, et al. (2010) Loss of beta-III spectrin leads to Purkinje cell dysfunction recapitulating the behavior and neuropathology of spinocerebellar ataxia type 5 in humans. *J Neurosci* 30:4857–4867.
4. Hourez R, et al. (2011) Aminopyridines correct early dysfunction and delay neurodegeneration in a mouse model of spinocerebellar ataxia type 1. *J Neurosci* 31: 11795–11807.
5. Dell'Orco JM, et al. (2015) Neuronal atrophy early in degenerative ataxia is a compensatory mechanism to regulate membrane excitability. *J Neurosci* 35:11292–11307.
6. Nakamura K, et al. (2001) SCA17, a novel autosomal dominant cerebellar ataxia caused by an expanded polyglutamine in TATA-binding protein. *Hum Mol Genet* 10: 1441–1448.
7. Dansithong W, et al. (2015) Ataxin-2 regulates RGS8 translation in a new BAC-SCA2 transgenic mouse model. *PLoS Genet* 11:e1005182.
8. Doss-Pepe EW, Stenroos ES, Johnson WG, Madura K (2003) Ataxin-3 interactions with rad23 and valosin-containing protein and its associations with ubiquitin chains and the proteasome are consistent with a role in ubiquitin-mediated proteolysis. *Mol Cell Biol* 23:6469–6483.
9. Burnett B, Li F, Pittman RN (2003) The polyglutamine neurodegenerative protein ataxin-3 binds polyubiquitylated proteins and has ubiquitin protease activity. *Hum Mol Genet* 12:3195–3205.
10. Iwaki A, et al. (2008) Heterozygous deletion of ITPR1, but not SUMF1, in spinocerebellar ataxia type 16. *J Med Genet* 45:32–35.
11. Marelli C, et al. (2011) SCA15 due to large ITPR1 deletions in a cohort of 333 white families with dominant ataxia. *Arch Neurol* 68:637–643.
12. Jackson M, et al. (2001) Modulation of the neuronal glutamate transporter EAAT4 by two interacting proteins. *Nature* 410:89–93.
13. Ikeda Y, et al. (2006) Spectrin mutations cause spinocerebellar ataxia type 5. *Nat Genet* 38:184–190.
14. Soriano P, Montgomery C, Geske R, Bradley A (1991) Targeted disruption of the c-src proto-oncogene leads to osteopetrosis in mice. *Cell* 64:693–702.
15. Stein PL, Vogel H, Soriano P (1994) Combined deficiencies of Src, Fyn, and Yes tyrosine kinases in mutant mice. *Genes Dev* 8:1999–2007.
16. Grant SG, et al. (1992) Impaired long-term potentiation, spatial learning, and hippocampal development in fyn mutant mice. *Science* 258:1903–1910.
17. Grant SG, Karl KA, Kiebler MA, Kandel ER (1995) Focal adhesion kinase in the brain: Novel subcellular localization and specific regulation by Fyn tyrosine kinase in mutant mice. *Genes Dev* 9:1909–1921.
18. Kuo G, Arnaud L, Kronstad-O'Brien P, Cooper JA (2005) Absence of Fyn and Src causes a reeler-like phenotype. *J Neurosci* 25:8578–8586.
19. Okada M, Nada S, Yamanashi Y, Yamamoto T, Nakagawa H (1991) CSK: A protein-tyrosine kinase involved in regulation of src family kinases. *J Biol Chem* 266: 24249–24252.
20. Zheng XM, Wang Y, Pallen CJ (1992) Cell transformation and activation of pp60c-src by overexpression of a protein tyrosine phosphatase. *Nature* 359:336–339.
21. Kapus A, Szászi K, Sun J, Rizoli S, Rotstein OD (1999) Cell shrinkage regulates Src kinases and induces tyrosine phosphorylation of cortactin, independent of the osmotic regulation of Na+/H+ exchangers. *J Biol Chem* 274:8093–8102.
22. Lu YM, Roder JC, Davidow J, Salter MW (1998) Src activation in the induction of long-term potentiation in CA1 hippocampal neurons. *Science* 279:1363–1367.
23. Imamura K, et al. (2017) The Src/c-Abl pathway is a potential therapeutic target in amyotrophic lateral sclerosis. *Sci Transl Med* 9:eaaf3962.
24. Kaufman AC, et al. (2015) Fyn inhibition rescues established memory and synapse loss in Alzheimer mice. *Ann Neurol* 77:953–971.
25. Pal R, et al. (2014) Src-dependent impairment of autophagy by oxidative stress in a mouse model of Duchenne muscular dystrophy. *Nat Commun* 5:4425.
26. Lee Y-G, Macoska JA, Korenchuk S, Pienta KJ (2002) MIM, a potential metastasis suppressor gene in bladder cancer. *Neoplasia* 4:291–294.
27. Yang C, Hoelzle M, Disanza A, Scita G, Svitkina T (2009) Coordination of membrane and actin cytoskeleton dynamics during filopodia protrusion. *PLoS One* 4: e5678–e5679.
28. Bershteyn M, Atwood SX, Woo W-M, Li M, Oro AE (2010) MIM and cortactin antagonism regulates ciliogenesis and hedgehog signaling. *Dev Cell* 19:270–283.
29. Quinones GA, Jin J, Oro AE (2010) I-BAR protein antagonism of endocytosis mediates directional sensing during guided cell migration. *J Cell Biol* 189:353–367.
30. Callahan CA, et al. (2004) MIM/BEG4, a Sonic hedgehog-responsive gene that potentiates Gli-dependent transcription. *Genes Dev* 18:2724–2729.
31. Ohnishi H, Murata Y, Okazawa H, Matozaki T (2011) Src family kinases: Modulators of neurotransmitter receptor function and behavior. *Trends Neurosci* 34:629–637.
32. Uruno T, et al. (2001) Activation of Arp2/3 complex-mediated actin polymerization by cortactin. *Nat Cell Biol* 3:259–266.
33. Wu H, Parsons JT (1993) Cortactin, an 80/85-kilodalton pp60src substrate, is a filamentous actin-binding protein enriched in the cell cortex. *J Cell Biol* 120:1417–1426.
34. Huang C, et al. (1997) Down-regulation of the filamentous actin cross-linking activity of cortactin by Src-mediated tyrosine phosphorylation. *J Biol Chem* 272:13911–13915.
35. Lynch DK, et al. (2003) A Cortactin-CD2-associated protein (CD2AP) complex provides a novel link between epidermal growth factor receptor endocytosis and the actin cytoskeleton. *J Biol Chem* 278:21805–21813.
36. Hensel N, Claus P (2018) The actin cytoskeleton in SMA and ALS: How does it contribute to motoneuron degeneration? *Neuroscientist* 24:54–72.

37. Yan Z, Kim E, Datta D, Lewis DA, Soderling SH (2016) Synaptic actin dysregulation, a convergent mechanism of mental disorders? *J Neurosci* 36:11411–11417.
38. Avery AW, Thomas DD, Hays TS (2017) β-III-spectrin spinocerebellar ataxia type 5 mutation reveals a dominant cytoskeletal mechanism that underlies dendritic arborization. *Proc Natl Acad Sci USA* 114:E9376–E9385.
39. Yu D, et al. (2011) Mice deficient in MIM expression are predisposed to lymphomagenesis. 31:3561–3568.
40. Saarikangas J, et al. (2011) Missing-in-metastasis MIM/MTSS1 promotes actin assembly at intercellular junctions and is required for integrity of kidney epithelia. *J Cell Sci* 124:1245–1255.
41. Saarikangas J, et al. (2015) MIM-induced membrane bending promotes dendritic spine initiation. *Dev Cell* 33:644–659.
42. Glassmann A, et al. (2007) Developmental expression and differentiation-related neuron-specific splicing of metastasis suppressor 1 (Mtss1) in normal and transformed cerebellar cells. *BMC Dev Biol* 7:111–115.
43. Nixdorf S, et al. (2004) Expression and regulation of MIM (Missing In Metastasis), a novel putative metastasis suppressor gene, and MIM-B, in bladder cancer cell lines. *Cancer Lett* 215:209–220.
44. Sistig T (2017) Mtss1 promotes maturation and maintenance of cerebellar neurons via splice variant-specific effects. *Brain Struct Funct* 222:2787–2805.
45. Fahrenkamp D, Herrmann O, Koschmieder S, Brummendorf TH, Schemionek M (2017) Mtss1(CSC156) mutant mice fail to display efficient Mtss1 protein depletion. *Leukemia* 31:1017–1019.
46. Guyenet SJ, et al. (2010) A simple composite phenotype scoring system for evaluating mouse models of cerebellar ataxia. *J Vis Exp,* 1787.
47. Dawson JC, Timpson P, Kalna G, Machesky LM (2011) Mtss1 regulates epidermal growth factor signaling in head and neck squamous carcinoma cells. *Oncogene* 31: 1781–1793.
48. Hara T, et al. (2006) Suppression of basal autophagy in neural cells causes neurodegenerative disease in mice. *Nature* 441:885–889.
49. Komatsu M, et al. (2006) Loss of autophagy in the central nervous system causes neurodegeneration in mice. *Nature* 441:880–884.
50. Kegel KB, et al. (2000) Huntingtin expression stimulates endosomal-lysosomal activity, endosome tubulation, and autophagy. *J Neurosci* 20:7268–7278.
51. Nixon RA, et al. (2005) Extensive involvement of autophagy in Alzheimer disease: An immuno-electron microscopy study. *J Neuropathol Exp Neurol* 64:113–122.
52. Nascimento-Ferreira I, et al. (2011) Overexpression of the autophagic beclin-1 protein clears mutant ataxin-3 and alleviates Machado-Joseph disease. *Brain* 134:1400–1415.
53. Ropolo A, et al. (2007) The pancreatitis-induced vacuole membrane protein 1 triggers autophagy in mammalian cells. *J Biol Chem* 282:37124–37133.
54. Gal J, Ström A-L, Kilty R, Zhang F, Zhu H (2007) p62 accumulates and enhances aggregate formation in model systems of familial amyotrophic lateral sclerosis. *J Biol Chem* 282:11068–11077.
55. Shakkottai VG, et al. (2011) Early changes in cerebellar physiology accompany motor dysfunction in the polyglutamine disease spinocerebellar ataxia type 3. *J Neurosci* 31: 13002–13014.
56. Canepari M, Ogden D (2003) Evidence for protein tyrosine phosphatase, tyrosine kinase, and G-protein regulation of the parallel fiber metabotropic slow EPSC of rat cerebellar Purkinje neurons. *J Neurosci* 23:4066–4071.
57. Walter JT, Alviña K, Womack MD, Chevez C, Khodakhah K (2006) Decreases in the precision of Purkinje cell pacemaking cause cerebellar dysfunction and ataxia. *Nat Neurosci* 9:389–397.
58. Cerminara NL, Rawson JA (2004) Evidence that climbing fibers control an intrinsic spike generator in cerebellar Purkinje cells. *J Neurosci* 24:4510–4517.
59. Womack M, Khodakhah K (2002) Active contribution of dendrites to the tonic and trimodal patterns of activity in cerebellar Purkinje neurons. *J Neurosci* 22:10603–10612.
60. Meera P, Pulst S, Otis T (2017) A positive feedback loop linking enhanced mGluR function and basal calcium in spinocerebellar ataxia type 2. *eLife* 6:e26377.
61. Porkka K, et al. (2008) Dasatinib crosses the blood-brain barrier and is an efficient therapy for central nervous system Philadelphia chromosome-positive leukemia. *Blood* 112:1005–1012.
62. Pulst SM, et al. (1996) Moderate expansion of a normally biallelic trinucleotide repeat in spinocerebellar ataxia type 2. *Nat Genet* 14:269–276.
63. Huynh DP, Maalouf M, Silva AJ, Schweizer FE, Pulst SM (2009) Dissociated fear and spatial learning in mice with deficiency of ataxin-2. *PLoS One* 4:e6235.
64. Elden AC, et al. (2010) Ataxin-2 intermediate-length polyglutamine expansions are associated with increased risk for ALS. *Nature* 466:1069–1075.
65. Lim C, Allada R (2013) ATAXIN-2 activates PERIOD translation to sustain circadian rhythms in Drosophila. *Science* 340:875–879.
66. Xu X, et al. (2014) Anti-miR182 reduces ovarian cancer burden, invasion, and metastasis: An in vivo study in orthotopic xenografts of nude mice. *Mol Cancer Ther* 13:1729–1739.
67. Wu W, et al. (2014) MicroRNA-135b regulates metastasis suppressor 1 expression and promotes migration and invasion in colorectal cancer. *Mol Cell Biochem* 388:249–259.
68. Zhou W, et al. (2012) MiR-135a promotes growth and invasion of colorectal cancer via metastasis suppressor 1 in vitro. *Acta Biochim Biophys Sin (Shanghai)* 44:838–846.
69. Kedmi M, et al. (2015) EGF induces microRNAs that target suppressors of cell migration: miR-15b targets MTSS1 in breast cancer. *Sci Signal* 8:ra29.
70. Jahid S, et al. (2012) miR-23a promotes the transition from indolent to invasive colorectal cancer. *Cancer Discov* 2:540–553.
71. Orr HT, et al. (1993) Expansion of an unstable trinucleotide CAG repeat in spinocerebellar ataxia type 1. *Nat Genet* 4:221–226.
72. Lam YC, et al. (2006) ATAXIN-1 interacts with the repressor Capicua in its native complex to cause SCA1 neuropathology. *Cell* 127:1335–1347.
73. Ingram M, et al. (2016) Cerebellar transcriptome profiles of ATXN1 transgenic mice reveal SCA1 disease progression and protection pathways. *Neuron* 89:1194–1207.
74. Lise S, et al. (2012) Recessive mutations in SPTBN2 implicate β-III spectrin in both cognitive and motor development. *PLoS Genet* 8:e1003074–e14.
75. Burright EN, et al. (1995) SCA1 transgenic mice: A model for neurodegeneration caused by an expanded CAG trinucleotide repeat. *Cell* 82:937–948.
76. Gonzalez-Quevedo R, Shoffer M, Horng L, Oro AE (2005) Receptor tyrosine phosphatase-dependent cytoskeletal remodeling by the hedgehog-responsive gene MIM/BEG4. *J Cell Biol* 168:453–463.
77. Alazami AM, et al. (2015) Accelerating novel candidate gene discovery in neurogenetic disorders via whole-exome sequencing of prescreened multiplex consanguineous families. *Cell Rep* 10:148–161.
78. Gennarino VA, et al. (2015) Pumilio1 haploinsufficiency leads to SCA1-like neurodegeneration by increasing wild-type Ataxin1 levels. *Cell* 160:1087–1098.
79. Gennarino VA, et al. (2018) A mild PUM1 mutation is associated with adult-onset ataxia, whereas haploinsufficiency causes developmental delay and seizures. *Cell* 172:924–936.e11.
80. Chen D, et al. (2012) Pumilio 1 suppresses multiple activators of p53 to safeguard spermatogenesis. *Curr Biol* 22:420–425.
81. Kedde M, et al. (2010) A Pumilio-induced RNA structure switch in p27-3′ UTR controls miR-221 and miR-222 accessibility. *Nat Cell Biol* 12:1014–1020.
82. Lei R, et al. (2014) Suppression of MIM by microRNA-182 activates RhoA and promotes breast cancer metastasis. *Oncogene* 33:1287–1296.
83. Wang Y, Arribas-Layton M, Chen Y, Lykke-Andersen J, Sen GL (2015) DDX6 orchestrates mammalian progenitor function through the mRNA degradation and translation pathways. *Mol Cell* 60:118–130.
84. Li C, Götz J (2017) Somatodendritic accumulation of Tau in Alzheimer's disease is promoted by Fyn-mediated local protein translation. *EMBO J* 36:3120–3138.
85. Park J, et al. (2013) RAS-MAPK-MSK1 pathway modulates ataxin 1 protein levels and toxicity in SCA1. *Nature* 498:325–331.
86. Rodríguez CI, et al. (2000) High-efficiency deleter mice show that FLPe is an alternative to Cre-loxP. *Nat Genet* 25:139–140.
87. Tang S-HE, Silva FJ, Tsark WMK, Mann JR (2002) A cre/loxP-deleter transgenic line in mouse strain 129S1/SvImJ. *Genesis* 32:199–202.
88. Zhang X-M, et al. (2004) Highly restricted expression of Cre recombinase in cerebellar Purkinje cells. *Genesis* 40:45–51.